

# Impurity-induced triple point fermions in twisted bilayer graphene

Aline Ramires<sup>1,2,\*</sup> and Jose L. Lado<sup>3</sup>

<sup>1</sup>*ICTP-SAIFR, International Centre for Theoretical Physics - South American Institute for Fundamental Research, São Paulo, SP, 01140-070, Brazil*

<sup>2</sup>*Instituto de Física Teórica - Universidade Estadual Paulista, São Paulo, SP, 01140-070, Brazil*

<sup>3</sup>*Institute for Theoretical Physics, ETH Zurich, 8093 Zurich, Switzerland*

(Dated: June 4, 2019)

Triple point fermions are elusive electronic excitations that generalize Dirac and Weyl modes beyond the conventional high energy paradigm. Yet, finding real materials naturally hosting these excitations at the Fermi energy has remained challenging. Here we show that twisted bilayer graphene is a versatile platform to realize robust triple point fermions in two dimensions. In particular, we establish that the introduction of localized impurities lifts one of the two degenerate Dirac cones, yielding triple point fermions at charge neutrality. Furthermore, we show that the valley polarization is preserved for certain impurity locations in the moire supercell for both weak and strong impurity potentials. We finally show that in the presence of interactions, a symmetry broken state with local magnetization can develop out of the triple point bands, which can be selectively controlled by electrostatic gating. Our results put forward twisted bilayer graphene as a simple solid-state platform to realize triple point fermions at charge neutrality, and demonstrate the non-trivial role of impurities in moire systems.

## I. INTRODUCTION

Topological semimetals have attracted a lot of attention in the past years, as they provide solid-state platforms to realize analogs of relativistic particles<sup>1,2</sup>, namely Dirac and Weyl fermions<sup>3</sup>, whose spinorial form stems from Lorentz invariance. However, space group symmetries in materials provide an even more versatile playground, as they impose only a subset of the symmetries inflicted by Lorentz invariance, enabling novel types of effective particles to emerge beyond the conventional high energy paradigm<sup>4-19</sup>. Among these possibilities, triple point fermions<sup>4,5,20-28</sup> are exotic excitations displaying unusual magneto-transport phenomena including large negative magneto-resistance and helical anomaly<sup>29-31</sup>, in contrast to the chiral anomaly observed in Weyl semimetals<sup>3</sup>. From the material science point of view, recent proposals suggest the presence of triple point fermions away from the Fermi energy in Heusler compounds<sup>20,32</sup>. Experimentally, angle-resolved photoemission spectroscopy (ARPES) measurements have observed triple point fermions<sup>13,14,18</sup>, but only weak signatures of the expected exotic transport phenomena could be observed given the distance of the triple points to the Fermi level<sup>22,30</sup>. Thus, materials displaying robust triple point fermions at the Fermi energy have remained elusive, frustrating the experimental exploration of their associated exotic properties.

Graphene is known for being an extremely clean platform to explore Dirac fermion phenomena, with two spin degenerate Dirac cones at each  $K$  point<sup>33</sup>. Engineering triple point fermions out of graphene by lifting the degeneracy of the Dirac points would require eliminating key symmetries, which usually leads to a shift of the cones or to a gapped spectrum. Introducing an additional level of complexity, graphene multilayers have the potential to enlarge the degeneracy of the Dirac cones, providing new

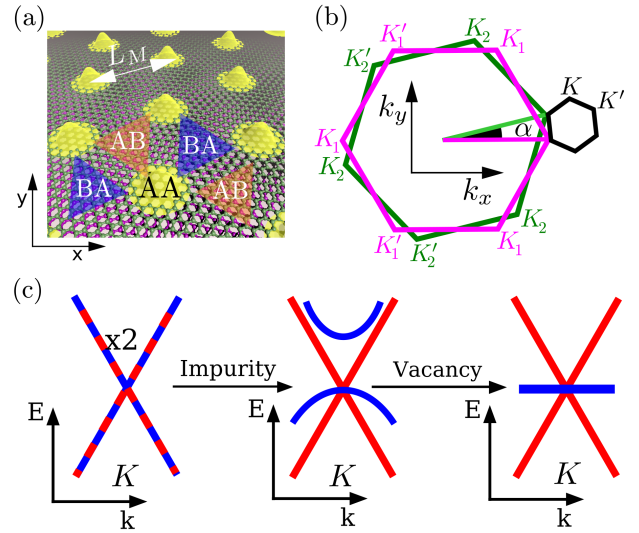


FIG. 1. (a) Perspective view of twisted bilayer graphene, highlighting the electronic density concentrated in the AA regions (yellow blobs), the AB/BA regions (orange/blue triangles), and the moire length  $L_M$ . (b) Brillouin zones for the first (pink) and second (green) layer, and the emergent moire Brillouin zone (black), with the respective  $K$  and  $K'$  points. (c) Sketch of the effects of a weak impurity and a vacancy on the degenerate low energy Dirac cones, with the generation of a triple point at the Fermi level.

routes for degeneracy lifting. Among them, twisted bilayer graphene (TBG) (Fig. 1(a)) is an especially promising candidate for displaying a band structure with four-fold degenerate Dirac cones in the reduced Brillouin zone (Fig. 1(b) and (c))<sup>34-36</sup>, providing a potential direction for the engineering of triple points by the controlled reduction of symmetries.

Here we show that impurities in TBG create robust

triple point fermions. This unexpected feature stems from the interplay of the Dirac point degeneracy and the local nature of the impurity, which gives rise to mass generation in one of the Dirac cones, creating a triple point at charge neutrality independently of the strength and location of the impurity. Furthermore, we show that the valley polarization of the triple point can be controlled by the location of the impurities in the moire supercell. The manuscript is organized as follows: in Sec. II we introduce the tight binding model for twisted bilayer graphene, as well as a procedure to compute the expectation value of the valley operator in real space. In Sec. III, we numerically show the presence of triple points for weak impurities and provide a low energy effective model which accounts for the triple point formation and discuss its robustness. We examine the vacancy limit, in Sec. IV. In Sec. V, we evaluate the effect of interactions in this triple point system, showing that electronic doping allows one to selectively control the symmetry broken phases. Finally, in Sec. VI we summarize our results and conclusions.

## II. TIGHT BINDING MODEL FOR TWISTED BILAYER GRAPHENE WITH LOCAL IMPURITIES

Here we focus on TBG superlattices with long moire wavelength, i.e. small twisting angles  $\alpha$  (see Fig. 1 (a)), but we would like to highlight that the presence of the triple point is independent of the magnitude of the twist angle, as discussed in detail in Appendix A. In the small angle regime, the low energy model consists of two sets of honeycomb-like bands with strongly renormalized Fermi velocity, which vanishes at the magic angle  $\alpha \approx 1^\circ$ <sup>37,38</sup>. We model TBG in the presence of impurities by the real space Hamiltonian of the form:

$$\mathcal{H} = \mathcal{H}_0 + \mathcal{W}, \quad (1)$$

where  $\mathcal{H}_0$  encodes the pristine TBG tight binding Hamiltonian<sup>39</sup>:

$$\mathcal{H}_0 = t \sum_{\langle i,j \rangle} c_i^\dagger c_j + \sum_{i,j} \bar{t}_\perp(\mathbf{r}_i, \mathbf{r}_j) c_i^\dagger c_j, \quad (2)$$

and  $\mathcal{W}$  describes a local impurity at site  $n$

$$\mathcal{W} = w c_n^\dagger c_n, \quad (3)$$

where  $c_i^\dagger$  ( $c_i$ ) is the fermionic creation (annihilation) operator at site  $i$ ,  $w$  is the impurity potential strength,  $t$  is the nearest neighbor hopping,  $\langle i, j \rangle$  indicates the sum over first neighbors, and  $\bar{t}_\perp(\mathbf{r}_i, \mathbf{r}_j)$  is the distance-dependent interlayer coupling taking a maximum value  $t_\perp$  for perfect stacking<sup>40</sup>. As a reference, the values of the parameters in graphene are  $t \approx 3$  eV and  $t_\perp \approx 300$  meV<sup>41</sup>. The previous Hamiltonian is defined in a moire unit cell with  $N = 4(3m_0^2 + 3m_0 + 1)$  sites, with  $m_0$  an integer, and the magic angle regime is reached for  $t_\perp/(tm_0) \approx 0.025$ .

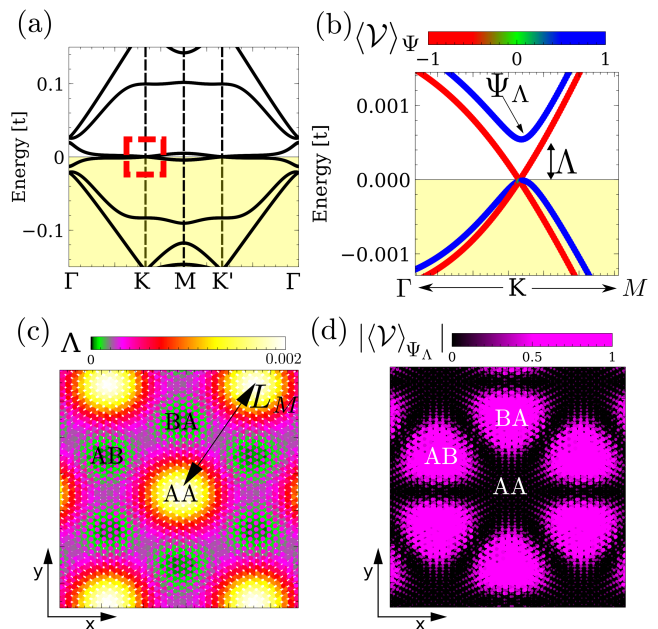


FIG. 2. (a) Band structure of twisted bilayer graphene with  $\alpha = 1.5^\circ$  in the presence of a weak impurity in the AB region. (b) A zoom at the K point, showing the valley polarization  $\langle \mathcal{V} \rangle_\Psi$  of each state (color gradient) and the emergence of a gap of magnitude  $\Lambda$ . (c) Map of the splitting  $\Lambda$  as a function of the impurity position. (d) Map of the valley polarization of  $\Psi_\Lambda$  at the K point, as a function of the impurity position. Here we took  $m_0 = 11$ ,  $t_\perp = 0.3t$  and  $w = 0.5t$ .

For the sake of simplicity here we omit the spin degree of freedom. It should be understood that for the spinful scenario the triple-point degeneracy is in fact six-fold.

In the absence of impurities,  $w = 0$ , the low energy spectra of the previous Hamiltonian consists of two Dirac cones at  $K$  and other two at  $K'$ <sup>35-38,42</sup>. This degeneracy can be understood by the folding of the cone at  $K_1$  from layer 1 and  $K'_2$  from layer 2 at the same  $K$  point in the moire Brillouin zone, as can be seen from Fig. 1 (b). Due to the approximate valley symmetry of the low energy graphene Hamiltonian, the states associated with each decoupled layer  $\ell$  in TBG can be labeled by their valley number  $\mathcal{V}_\ell$ . In a real space tight-binding formalism, such valley flavor can be computed using the valley operator:

$$\mathcal{V}_\ell = \frac{i}{3\sqrt{3}} \sum_{\langle\langle i,j \rangle\rangle \in \ell} \eta_{ij} \sigma_z^{ij} c_i^\dagger c_j, \quad (4)$$

where  $\langle\langle i, j \rangle\rangle$  denotes second neighbor sites,  $\eta_{ij} = \pm 1$  is for clockwise or anticlockwise hopping, and  $\sigma_z^{ij}$  is a Pauli matrix associated with the sublattice degree of freedom<sup>43,44</sup>. The interlayer hopping couples opposite valleys between the two layers, giving rise to a new quantum number  $\mathcal{V} = \mathcal{V}_1 - \mathcal{V}_2$ , which is conserved in the absence of impurities. The addition of impurities generally introduces inter-valley scattering, and therefore it is interesting to track the valley polarization of the states.

### III. WEAK IMPURITY LIMIT

We first consider the case of a weak impurity in twisted bilayer graphene. When the local impurity potential is turned on,  $w \neq 0$ , the four-fold degeneracy of the states at  $K$  and  $K'$  is lifted, giving rise to triple points at the Fermi level, as shown in Fig. 2 (a) and (b), independently of the position of the impurity in the moire pattern. The location of the impurity controls the splitting  $\Lambda$  between the triple point and the higher lying state  $\Psi_\Lambda$ . In particular, Fig. 2 (c) shows that impurities located in the AA regions create larger splittings. This can be understood from the larger amplitude of the wave functions in these regions<sup>35–38,42,45</sup>, as schematically shown in Fig. 1(a). Interestingly, although a local impurity would be expected to give rise to inter-valley mixing between the degenerate Dirac points, we observe that the states associated with the triple point and  $\Psi_\Lambda$  remain valley polarized for impurities located in the AB/BA regions, as shown in Fig. 2 (d).

#### A. Low energy effective model

The robustness of the triple point is guaranteed by the effective valley quantum number and the properties of the emergent orbitals at low energies. It can be understood from the consideration of the band degeneracy of pristine TBG. The band structure is displayed in Fig. 3 (a), with two double degenerate bands crossing the Fermi level in the  $\Gamma - K - M$  direction<sup>46</sup>. We can label the eigenstates associated with the branches  $E_{1\mathbf{k}}$  as  $\Psi_{1\mathbf{k}}$  and  $\Psi_{\bar{1}\mathbf{k}}$ , and the other two associated with  $E_{2\mathbf{k}} = -E_{1\mathbf{k}}$  as  $\Psi_{2\mathbf{k}}$  and  $\Psi_{\bar{2}\mathbf{k}}$ . These wave functions have weight in all microscopic degrees of freedom, layer and sublattice, such that these are expected to have a finite amplitude at a generic impurity site. Focusing on the first degenerate set, an impurity introduces a coupling between the eigenstates of pristine TBG such that the Hamiltonian in the eigenbasis  $(\Psi_{1\mathbf{k}}, \Psi_{\bar{1}\mathbf{k}})$  can be written as  $H_1(\mathbf{k}) = \begin{pmatrix} E_{1\mathbf{k}} + v_1 & \sqrt{v_{\bar{1}}v_1} \\ \sqrt{v_{\bar{1}}v_1} & E_{1\mathbf{k}} + v_{\bar{1}} \end{pmatrix}$ , where  $v_1$  and  $v_{\bar{1}}$  stand for the coupling of the impurity to the respective state,  $v_i = w|\Psi_{i\mathbf{k}}(\mathbf{r}_n)|^2$ . This eigenproblem has solution  $\phi_{1\mathbf{k}}$  with  $E_{1\mathbf{k}}$  and  $\phi_{\bar{1}\mathbf{k}}$  with  $E_{1\mathbf{k}} + v_1 + v_{\bar{1}}$ . Note that  $\phi_{1\mathbf{k}}$  remains at its original energy, indicating that it has zero amplitude at the impurity site and is therefore blind to its presence, while  $\phi_{\bar{1}\mathbf{k}}$  couples to the impurity and is shifted in energy. An analogous construction can be made for states  $\Psi_{2\mathbf{k}}$  and  $\Psi_{\bar{2}\mathbf{k}}$ , such that in the appropriate combination, one of the states decouples from the impurity site, such that  $\phi_{1\mathbf{k}}$  and  $\phi_{2\mathbf{k}}$  give rise to two bands which do not change in presence of the impurity.

We now focus on the  $K$  point, at which all low lying bands become degenerate. At this point, we can choose to write the eigenstates in a basis which is valley polarized. From the numerical analysis, we infer that this basis can, in fact, be written as  $\Psi^\dagger = (\phi_{1\mathbf{k}}^\dagger, \phi_{\bar{1}\mathbf{k}}^\dagger, \phi_{2\mathbf{k}}^\dagger, \phi_{\bar{2}\mathbf{k}}^\dagger)$ ,

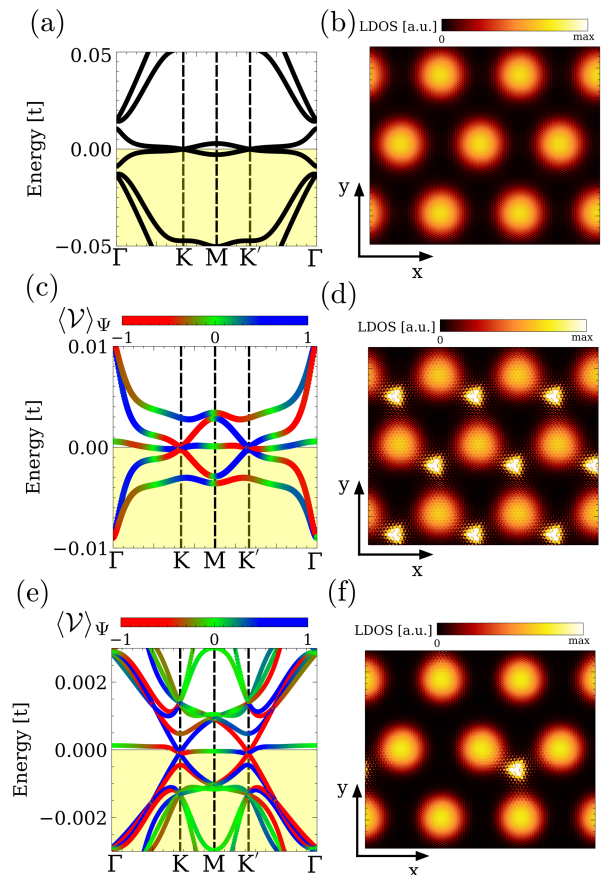


FIG. 3. Band structure of pristine twisted bilayer graphene at  $\alpha = 1.5^\circ$ , and (b) local density of states at charge neutrality  $E = 0$ . (c) Band structure with a single impurity per moire supercell, together with the (d) local density of states, showing the emergence of zero modes around the impurity. (e) Band structure for a single vacancy in a  $2 \times 2$  supercell, and (f) spatial density of states. We took  $m_0 = 22$  and  $t_\perp = 0.15t$  for all panels.

in terms of the eigenstates discussed in the previous paragraph. In this basis the valley operator yields  $\mathcal{V} = \text{diag}(+1, +1, -1, -1)$ , and the effective Hamiltonian around the  $K$  point is of the form:

$$H^{eff}(K + \mathbf{k}) = \begin{pmatrix} \Lambda_1 & \bar{k} & 0 & \sqrt{\Lambda_1\Lambda_2} \\ \bar{k}^* & 0 & 0 & 0 \\ 0 & 0 & 0 & \bar{k}^* \\ \sqrt{\Lambda_1\Lambda_2} & 0 & \bar{k} & \Lambda_2 \end{pmatrix} \quad (5)$$

where  $\bar{k} = \bar{v}_F(k_x + ik_y)$ ,  $\bar{v}_F$  is the renormalized Fermi velocity, and  $\Lambda_i = v_i + v_{\bar{i}}$ . The effective Hamiltonian at  $K'$  follows from time reversal symmetry. In the absence of impurities,  $\Lambda_{1,2} = 0$ , the doubly degenerate Dirac dispersion is found. In the presence of an impurity,  $\Lambda_{1,2} \neq 0$ , the effective Hamiltonian has eigenvalues  $\pm|\bar{k}|$  and  $\frac{1}{2}(\Lambda \pm \sqrt{4|\bar{k}|^2 + \Lambda^2})$ , where  $\Lambda = \Lambda_1 + \Lambda_2$ . Note that at the  $K$  point ( $\bar{k} = 0$ ) the eigenvalues are  $\{0, 0, 0, \Lambda\}$ ,



making the triple point explicit and associating the splitting to the magnitude of the impurity potential as  $\Lambda \sim w$ . In this generic scenario, states with different valley number are mixed. Note that in the case  $\Lambda_1 \neq 0$  and  $\Lambda_2 = 0$ , a triple point emerges with well defined valley number, since  $[\mathcal{V}, H^{eff}] = 0$ , as shown in Fig. 2 (b), which happens for impurities in the AB/BA regions, as mapped in Fig. 2 (d). This valley polarization for impurities in the AB/BA regions can be inferred from the properties of the Wannier wave functions in real space, as shown, for example, in Ref. 35.

#### IV. THE VACANCY LIMIT

We now move on to consider the case of vacancy effects<sup>47–55</sup>, namely,  $w \rightarrow \infty$ . This limit is especially attractive because it can be achieved by adsorbed hydrogen atoms<sup>56</sup>. Recent experiments have shown that it is possible to manipulate<sup>57</sup> and even automatize the manipulation<sup>58</sup> of hydrogen atoms with atomic precision by scanning tunneling microscope. A vacancy in monolayer graphene is known to give rise to a zero mode at charge neutrality, according to Lieb's theorem<sup>59</sup>. In TBG, this zero mode will, however, coexist in energy with the nearly flat honeycomb-like bands of Fig. 3 (a) and (b), and therefore it is expected to heavily hybridize with them. Interestingly, as shown in Fig. 3 (c), the hybridization of the vacancy mode with the honeycomb-like bands lifts one of the Dirac cones and generates a flat band. Moreover, even though vacancies are expected to create strong inter-valley scattering, we find that the remaining Dirac cones are perfectly valley polarized when the vacancy is located at the AB/BA regions, see Fig. 3 (c) and (d) and Fig. 3 (e) and (f), similarly to the weak impurity scenario above. The weak and strong potential limits can actually be continuously connected by ramping up the parameter  $w$ . In this process, it is observed that the  $K$  point always displays a triple point, two of the bands remain rigid, and the quadratic band pinned to the Fermi level evolves smoothly towards a flat band. As the potential is increased, part of the electronic density drifts from the AA regions to the location of the impurity. This phenomenology is observed to be independent of the density of vacancies per unit cell, as shown in the calculation for a 2x2 supercell in Fig. 3 (e) and (f)<sup>60</sup>.

#### V. INTERACTION EFFECTS

It is important to note that this discussion relied on a single particle picture. However, the large density of states associated with these nearly flat bands suggests that, at low temperatures, a symmetry broken state develops due to interactions<sup>36,61–64</sup>. To account for the effect of electronic interactions, we make explicit the spin degree of freedom in Eq. 1 and introduce an interaction term of the form  $H_U = U \sum_i n_{i\uparrow} n_{i\downarrow}$ , where  $n_{i\sigma}$

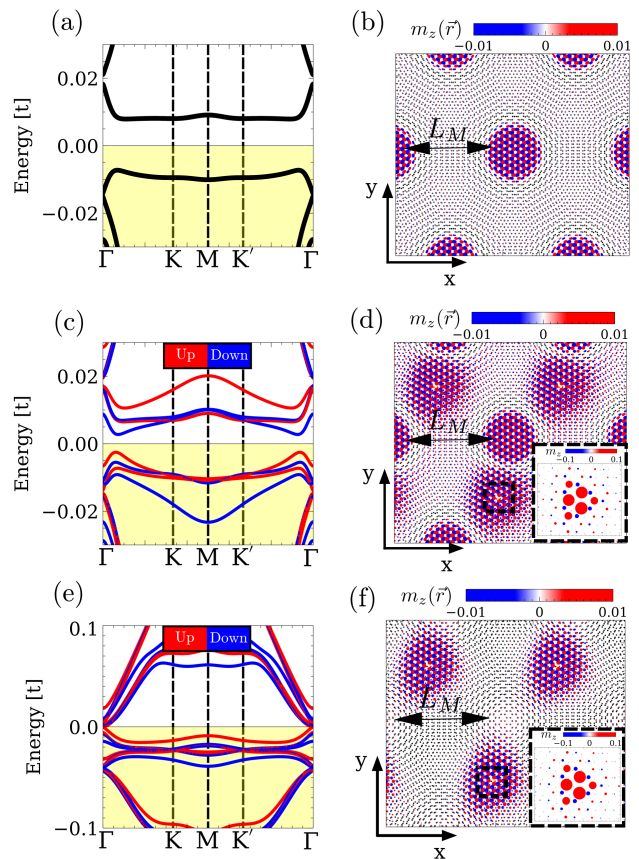


FIG. 4. Self-consistent band structure after including interactions for (a) charge neutral pristine twisted bilayer graphene, together with its (b) ground state magnetization. Self-consistent band structure of (c) twisted bilayer graphene with a single vacancy in the AB region, together with its (d) ground state magnetization. (e) The band structure and (f) magnetization with a filling of four electrons per unit cell with respect to charge neutrality. Note the different maximum values in (d) and (f) and their inset. We took  $m_0 = 11$ ,  $t_{\perp} = 0.3t$  and  $U = 2t$  for all panels.

counts the number of electrons with spin  $\sigma = \{\uparrow, \downarrow\}$  at site  $i$ <sup>45,61,65,66</sup>. We use a mean field ansatz of the form  $H_U \approx U \sum_i \langle n_{i\uparrow} \rangle n_{i\downarrow} + n_{i\uparrow} \langle n_{i\downarrow} \rangle - \langle n_{i\uparrow} \rangle \langle n_{i\downarrow} \rangle$ , with the expectation values determined self-consistently, allowing for a local ground state magnetization  $m_i^z = \langle n_{i\uparrow} \rangle - \langle n_{i\downarrow} \rangle$ . For pristine TBG at half filling, Figs. 4 (a) and (b) show that interactions drive the system into an insulating state with antiferromagnetic order in the AA regions<sup>45,61,67,68</sup>. A more interesting scenario takes place in the presence of a vacancy in an AB region of TBG, in which case electronic interactions create a localized magnetic moment<sup>47–54</sup>. As shown in Figs. 4 (c) and (d), the impurity state is not detrimental to the opening of a gap and the associated antiferromagnetic ordering of the AA regions, even though the magnetization associated with the impurity states is one order of magnitude larger than the staggered magnetization in the AA regions (see in-



set). As a result of the weak antiferromagnetism in the AA regions, doping quenches the antiferromagnetic order, while the magnetization around the vacancy survives. This can be clearly seen in Figs. 4 (e) and (f), where we consider a doping of four extra electrons per unit cell, which fills the low energy bands up to their edge. In fact, this phenomenology holds up to chemical potentials of the order of the exchange splitting  $\sim 30$  meV<sup>49,57</sup>, much bigger than the  $\sim 8$  meV bandwidth of the nearly flat bands<sup>35,36,38,42</sup>. As a result, at low temperatures, these localized magnetic moments may coexist with other phases found in the bilayer such as superconducting<sup>69</sup>, strange metal phases<sup>70</sup> or anomalous Hall states<sup>71</sup>.

In the case of larger angles, the Dirac cone states are not expected to have an electronic instability due to their substantial Fermi velocity. As a result, the ground state at half filling will be defined by an instability driven only by the impurity bands. These aspects are discussed in detail in Appendix B.

## VI. CONCLUSIONS

To summarize, we have established that impurities in small-angle twisted bilayer graphene give rise to robust triple point fermions at the charge neutrality point, independently of the impurity potential and its location. We have shown that the triple point modes can be valley polarized for defects located in the AB and BA regions, providing a route to engineer triple-point fermions with an additional quantized degree of freedom. In the presence of interactions, the triple points can be lifted by the development of magnetic order, introducing the possibility of engineering correlated states of triple point fermions in twisted bilayer graphene. Our results put forward a new mechanism to generate triple-points in graphene systems, providing a starting point to study their intrinsic properties and interplay with additional emergent states in twisted bilayers.

## ACKNOWLEDGMENTS

We would like to thank C. Timm, D. F. Agterberg, P. Brydon, H. Menke, T. M. R. Wolf, O. Zilberberg, G. Blatter, W. Chen, B. Amorim, F. Guinea, and E. V. Castro for helpful discussions. AR acknowledges financial support from FAPESP JP project (2018/04955-9) and fellowship (2018/18287-8), and Fundunesp/Simons Foundation (2338-2014 CCP). AR is also grateful for the hospitality of the Pauli Centre of ETH Zurich. J.L.L acknowledges financial support from the ETH Fellowship program and from the JSPS Core-to-Core program ‘‘Oxide Superspin’’ international network.

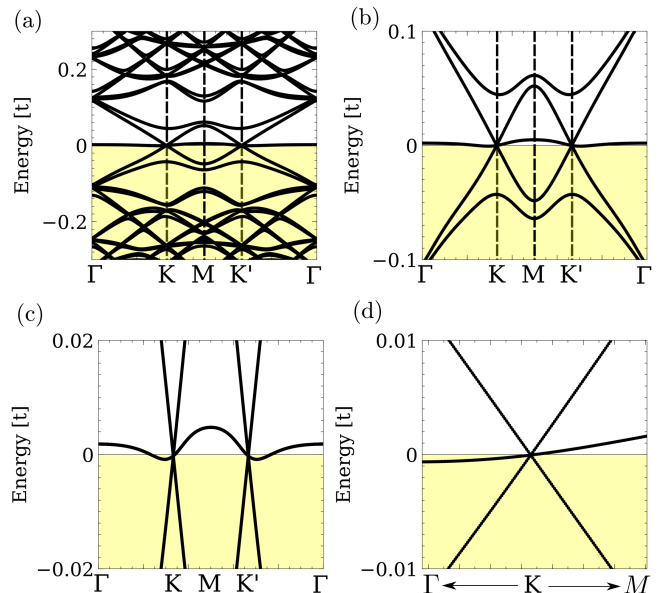


FIG. 5. (a) Band structure of twisted bilayer graphene with a vacancy in the AB region, for a twisting angle of  $\alpha \approx 3^\circ$  between the two layers. (b), (c) A zoom closer to the Fermi energy of (a) the band structure, and (d) a zoom close to the  $K$  point highlighting the triple crossing. We took  $m_0 = 11$  and  $t_\perp = 0.12t$ .

## Appendix A: Triple points for larger twisting angles

Above we focused on a small twisting angle,  $\alpha \approx 1.5^\circ$ , in which case the Dirac cones show a highly reduced Fermi velocity. In this scenario, in the presence of a vacancy, the system presented two types of localized modes, i.e., the vacancy mode and the nearly flat honeycomb band, forming a triple point at  $K$ .

The emergence of a triple point is not a unique feature of small angles. Here we show in Fig. 5 and 6 the band structure for angle  $\alpha \approx 3^\circ$  and  $\alpha \approx 9.5^\circ$ , respectively. Both structures show the emergence of a flat band, with a triple point crossing. In comparison with the case  $\alpha \approx 1.5^\circ$ , the Dirac cones for larger angles show a much higher Fermi velocity, a feature that does not affect the presence of the triple point. In order to show the robustness of the triple point within the tight-binding calculation, we also show figures which zoom in energy and around the  $K$  point for both angles.

## Appendix B: Interaction effects for $\alpha \approx 3^\circ$

In the case of larger angles shown above, the Dirac cone states are not expected to have an electronic instability due to their substantial Fermi velocity. As a result, the ground state at half filling will be defined by an instability driven only by the impurity bands, different than the one presented for  $\alpha \approx 1.5^\circ$  in the main text, where both flat Dirac cones and impurity bands contribute to the

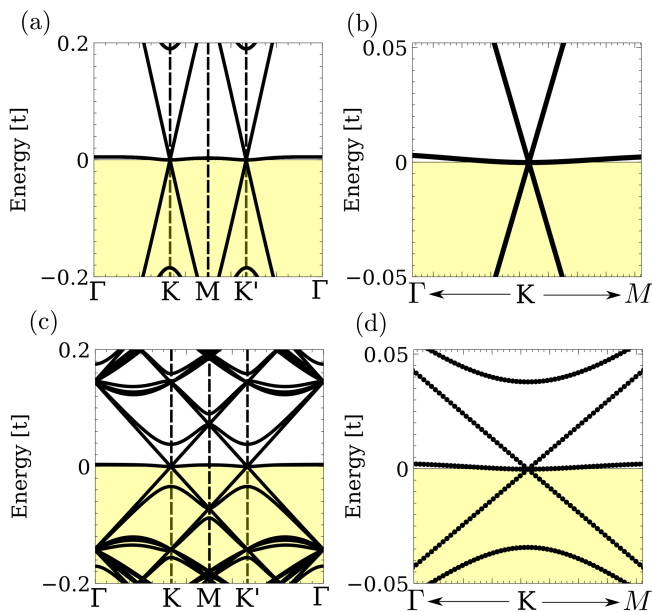


FIG. 6. (a) Band structure for twisted bilayer graphene at an angle  $\alpha \approx 9.5^\circ$  with one vacancy per moire unit cell, showing the existence of triple point crossing even at large angles (zoom in (b)). (c) Band structure for  $\alpha \approx 9.5^\circ$ , with one vacancy for a  $4 \times 4$  moire supercell, showing the persistence of triple point crossings (zoom in (d)).

instability.

Here we focus on the vacancy case for  $\alpha \approx 3^\circ$ , which presents a nearly flat band coexisting with a Dirac cone. For larger angles the electronic instability only takes place in the vacancy flat band, giving rise to a net magnetic moment of  $1\mu_B$  per unit cell as shown in Fig. 7. In particular, we show in the different panels of Fig. 7 that the electronic structure of the system is qualitatively similar for the different values of  $U$  ranging from  $U = t$  to  $U = 2t$ . It is particularly evident that the vacancy states are highly polarized, while the Dirac cones are split and shifted, what can only be clearly observed from Fig. 7

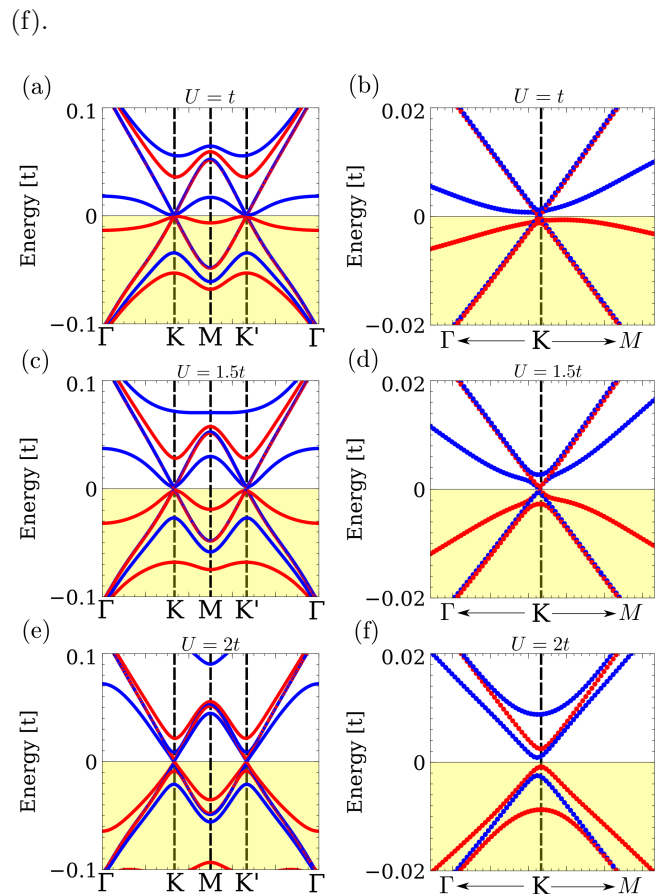


FIG. 7. Selfconsistent band structure for twisted bilayer graphene with a vacancy in the AB region, for an angle  $\alpha \approx 3^\circ$ , for (a)  $U = t$ , (c)  $U = 1.5t$  and (e)  $U = 2t$ , with (b), (d), and (f) the respective zooms around the original Dirac point. The higher interaction, the larger the exchange splitting of the vacancy bands. The color red/blue denotes the expectation value of  $S_z = \pm 1$ . We took  $m_0 = 11$  and  $t_\perp = 0.12t$  for all panels.

\* aline.ramires@ictp-saifr.org

<sup>1</sup> B. Yan and C. Felser, Annual Review of Condensed Matter Physics **8**, 337 (2017).

<sup>2</sup> A. A. Burkov, Nature Materials **15**, 1145 (2016).

<sup>3</sup> N. P. Armitage, E. J. Mele, and A. Vishwanath, Rev. Mod. Phys. **90**, 015001 (2018).

<sup>4</sup> Z. Zhu, G. W. Winkler, Q. S. Wu, J. Li, and A. A. Soluyanov, Phys. Rev. X **6**, 031003 (2016).

<sup>5</sup> C.-H. Cheung, R. C. Xiao, M.-C. Hsu, H.-R. Fuh, Y.-C. Lin, and C.-R. Chang, New Journal of Physics **20**, 123002 (2018).

<sup>6</sup> X. Zhang, Z.-M. Yu, X.-L. Sheng, H. Y. Yang, and S. A. Yang, Phys. Rev. B **95**, 235116 (2017).

<sup>7</sup> B. Bradlyn, L. Elcoro, J. Cano, M. G. Vergniory, Z. Wang, C. Felser, M. I. Aroyo, and B. A. Bernevig, Nature **547**,

298 EP (2017).

<sup>8</sup> B. J. Wieder, Y. Kim, A. M. Rappe, and C. L. Kane, Phys. Rev. Lett. **116**, 186402 (2016).

<sup>9</sup> T. Bzdušek, Q. Wu, A. Rüegg, M. Sigrist, and A. A. Soluyanov, Nature **538**, 75 (2016).

<sup>10</sup> Z. Wang, A. Alexandradinata, R. J. Cava, and B. A. Bernevig, Nature **532**, 189 (2016).

<sup>11</sup> A. A. Soluyanov, D. Gresch, Z. Wang, Q. Wu, M. Troyer, X. Dai, and B. A. Bernevig, Nature **527**, 495 (2015).

<sup>12</sup> J.-P. Sun, D. Zhang, and K. Chang, Phys. Rev. B **96**, 045121 (2017).

<sup>13</sup> J.-Z. Ma, J.-B. He, Y.-F. Xu, B. Q. Lv, D. Chen, W.-L. Zhu, S. Zhang, L.-Y. Kong, X. Gao, L.-Y. Rong, Y.-B. Huang, P. Richard, C.-Y. Xi, E. S. Choi, Y. Shao, Y.-L. Wang, H.-J. Gao, X. Dai, C. Fang, H.-M. Weng, G.-

- F. Chen, T. Qian, and H. Ding, *Nature Physics* **14**, 349 (2018).
- <sup>14</sup> B. Q. Lv, Z.-L. Feng, Q.-N. Xu, X. Gao, J.-Z. Ma, L.-Y. Kong, P. Richard, Y.-B. Huang, V. N. Strocov, C. Fang, H.-M. Weng, Y.-G. Shi, T. Qian, and H. Ding, *Nature* **546**, 627 (2017).
- <sup>15</sup> T. Kawakami, T. Okamura, S. Kobayashi, and M. Sato, *Phys. Rev. X* **8**, 041026 (2018).
- <sup>16</sup> M. Ezawa, *Phys. Rev. B* **95**, 205201 (2017).
- <sup>17</sup> S. A. Owerre, *EPL (Europhysics Letters)* **120**, 57002 (2017).
- <sup>18</sup> D. Takane, Z. Wang, S. Souma, K. Nakayama, T. Nakamura, H. Oinuma, Y. Nakata, H. Iwasawa, C. Cacho, T. Kim, K. Horiba, H. Kumigashira, T. Takahashi, Y. Ando, and T. Sato, *Phys. Rev. Lett.* **122**, 076402 (2019).
- <sup>19</sup> J. Kruthoff, J. de Boer, J. van Wezel, C. L. Kane, and R.-J. Slager, *Phys. Rev. X* **7**, 041069 (2017).
- <sup>20</sup> H. Yang, J. Yu, S. S. P. Parkin, C. Felser, C.-X. Liu, and B. Yan, *Phys. Rev. Lett.* **119**, 136401 (2017).
- <sup>21</sup> C. Shekhar, Y. Sun, N. Kumar, M. Nicklas, K. Manna, V. Suess, O. Young, I. Leermakers, T. Foerster, M. Schmidt, L. Muechler, P. Werner, W. Schnelle, U. Zeitler, B. Yan, S. S. P. Parkin, and C. Felser, *arXiv e-prints*, arXiv:1703.03736 (2017), arXiv:1703.03736 [cond-mat.mtrl-sci].
- <sup>22</sup> W. Gao, X. Zhu, F. Zheng, M. Wu, J. Zhang, C. Xi, P. Zhang, Y. Zhang, N. Hao, W. Ning, and M. Tian, *Nature Communications* **9**, 3249 (2018).
- <sup>23</sup> J. Wang, X. Sui, W. Shi, J. Pan, S. Zhang, F. Liu, S.-H. Wei, Q. Yan, and B. Huang, *Phys. Rev. Lett.* **119**, 256402 (2017).
- <sup>24</sup> Y. Xia and G. Li, *Phys. Rev. B* **96**, 241204 (2017).
- <sup>25</sup> P.-J. Guo, H.-C. Yang, K. Liu, and Z.-Y. Lu, *Phys. Rev. B* **98**, 045134 (2018).
- <sup>26</sup> F. Hütt, A. Yaresko, M. B. Schilling, C. Shekhar, C. Felser, M. Dressel, and A. V. Pronin, *Phys. Rev. Lett.* **121**, 176601 (2018).
- <sup>27</sup> J. Kim, H.-S. Kim, and D. Vanderbilt, *Phys. Rev. B* **98**, 155122 (2018).
- <sup>28</sup> N. J. Ghimire, M. A. Khan, A. S. Botana, J. S. Jiang, and J. F. Mitchell, *Phys. Rev. Materials* **2**, 081201 (2018).
- <sup>29</sup> H. Weng, C. Fang, Z. Fang, and X. Dai, *Phys. Rev. B* **93**, 241202 (2016).
- <sup>30</sup> J. B. He, D. Chen, W. L. Zhu, S. Zhang, L. X. Zhao, Z. A. Ren, and G. F. Chen, *Phys. Rev. B* **95**, 195165 (2017).
- <sup>31</sup> G. Chang, S.-Y. Xu, S.-M. Huang, D. S. Sanchez, C.-H. Hsu, G. Bian, Z.-M. Yu, I. Belopolski, N. Alidoust, H. Zheng, T.-R. Chang, H.-T. Jeng, S. A. Yang, T. Neupert, H. Lin, and M. Z. Hasan, *Scientific Reports* **7**, 1688 (2017).
- <sup>32</sup> C. K. Barman, C. Mondal, B. Pathak, and A. Alam, *Phys. Rev. B* **99**, 045144 (2019).
- <sup>33</sup> T. Wehling, A. Black-Schaffer, and A. Balatsky, *Advances in Physics* **63**, 1 (2014), <https://doi.org/10.1080/00018732.2014.927109>.
- <sup>34</sup> J. M. B. Lopes dos Santos, N. M. R. Peres, and A. H. Castro Neto, *Phys. Rev. B* **86**, 155449 (2012).
- <sup>35</sup> M. Koshino, N. F. Q. Yuan, T. Koretsune, M. Ochi, K. Kuroki, and L. Fu, *Phys. Rev. X* **8**, 031087 (2018).
- <sup>36</sup> J. Kang and O. Vafek, *Phys. Rev. X* **8**, 031088 (2018).
- <sup>37</sup> J. M. B. Lopes dos Santos, N. M. R. Peres, and A. H. Castro Neto, *Phys. Rev. Lett.* **99**, 256802 (2007).
- <sup>38</sup> R. Bistritzer and A. H. MacDonald, *Proceedings of the National Academy of Sciences* **108**, 12233 (2011).
- <sup>39</sup> A. O. Sboychakov, A. L. Rakhmanov, A. V. Rozhkov, and F. Nori, *Phys. Rev. B* **92**, 075402 (2015).
- <sup>40</sup> We take  $\bar{t}_\perp(\mathbf{r}_i, \mathbf{r}_j) = t_\perp \frac{(z_i - z_j)^2}{|\mathbf{r}_i - \mathbf{r}_j|^2} e^{-\beta(|\mathbf{r}_i - \mathbf{r}_j| - d)}$ , where for simplicity we take  $d = 3a$  the interlayer distance,  $\beta = 3/a$  with  $a$  the carbon-carbon distance.
- <sup>41</sup> E. McCann and M. Koshino, *Reports on Progress in Physics* **76**, 056503 (2013).
- <sup>42</sup> H. C. Po, L. Zou, A. Vishwanath, and T. Senthil, *Phys. Rev. X* **8**, 031089 (2018).
- <sup>43</sup> A. Ramires and J. L. Lado, *Phys. Rev. Lett.* **121**, 146801 (2018).
- <sup>44</sup> E. Colomé and M. Franz, *Phys. Rev. Lett.* **120**, 086603 (2018).
- <sup>45</sup> L. A. Gonzalez-Arraga, J. L. Lado, F. Guinea, and P. San-Jose, *Phys. Rev. Lett.* **119**, 107201 (2017).
- <sup>46</sup> The degeneracy in the  $\Gamma - M$  direction is broken already in the pristine system.
- <sup>47</sup> E. J. Duplock, M. Scheffler, and P. J. D. Lindan, *Phys. Rev. Lett.* **92**, 225502 (2004).
- <sup>48</sup> O. V. Yazyev, *Reports on Progress in Physics* **73**, 056501 (2010).
- <sup>49</sup> O. V. Yazyev and L. Helm, *Phys. Rev. B* **75**, 125408 (2007).
- <sup>50</sup> D. W. Boukhvalov, M. I. Katsnelson, and A. I. Lichtenstein, *Phys. Rev. B* **77**, 035427 (2008).
- <sup>51</sup> J. J. Palacios, J. Fernández-Rossier, and L. Brey, *Phys. Rev. B* **77**, 195428 (2008).
- <sup>52</sup> N. A. García-Martínez, J. L. Lado, D. Jacob, and J. Fernández-Rossier, *Phys. Rev. B* **96**, 024403 (2017).
- <sup>53</sup> F. J. Sousa, B. Amorim, and E. V. Castro, *arXiv e-prints*, arXiv:1901.08614 (2019), arXiv:1901.08614 [cond-mat.mes-hall].
- <sup>54</sup> K. Ulman and S. Narasimhan, *Phys. Rev. B* **89**, 245429 (2014).
- <sup>55</sup> M. M. Ugeda, I. Brihuega, F. Guinea, and J. M. Gómez-Rodríguez, *Phys. Rev. Lett.* **104**, 096804 (2010).
- <sup>56</sup> I. Brihuega and F. Yndurain, *The Journal of Physical Chemistry B* **122**, 595 (2017).
- <sup>57</sup> H. Gonzalez-Herrero, J. M. Gomez-Rodriguez, P. Mallet, M. Moaied, J. J. Palacios, C. Salgado, M. M. Ugeda, J.-Y. Veullen, F. Yndurain, and I. Brihuega, *Science* **352**, 437 (2016).
- <sup>58</sup> M. Møller, S. P. Jarvis, L. Guérinet, P. Sharp, R. Woolley, P. Rahe, and P. Moriarty, *Nanotechnology* **28**, 075302 (2017).
- <sup>59</sup> V. M. Pereira, J. M. B. Lopes dos Santos, and A. H. Castro Neto, *Phys. Rev. B* **77**, 115109 (2008).
- <sup>60</sup> Substantial second neighbor hopping adds a dispersion to the vacancy band yet preserving the triple point.
- <sup>61</sup> A. O. Sboychakov, A. V. Rozhkov, A. L. Rakhmanov, and F. Nori, *Phys. Rev. Lett.* **120**, 266402 (2018).
- <sup>62</sup> Y. Cao, V. Fatemi, A. Demir, S. Fang, S. L. Tomarken, J. Y. Luo, J. D. Sanchez-Yamagishi, K. Watanabe, T. Taniguchi, E. Kaxiras, R. C. Ashoori, and P. Jarillo-Herrero, *Nature* **556**, 80 (2018).
- <sup>63</sup> A. Thomson, S. Chatterjee, S. Sachdev, and M. S. Scheurer, *Phys. Rev. B* **98**, 075109 (2018).
- <sup>64</sup> C. Xu and L. Balents, *Phys. Rev. Lett.* **121**, 087001 (2018).
- <sup>65</sup> F. Finocchiaro, F. Guinea, and P. San-Jose, *2D Materials* **4**, 025027 (2017).
- <sup>66</sup> T. O. Wehling, E. Şaşıoğlu, C. Friedrich, A. I. Lichtenstein, M. I. Katsnelson, and S. Blügel, *Phys. Rev. Lett.* **106**, 236805 (2011).



- <sup>67</sup> S. Saremi, Phys. Rev. B **76**, 184430 (2007).
- <sup>68</sup> C.-C. Liu, L.-D. Zhang, W.-Q. Chen, and F. Yang, Phys. Rev. Lett. **121**, 217001 (2018).
- <sup>69</sup> Y. Cao, V. Fatemi, S. Fang, K. Watanabe, T. Taniguchi, E. Kaxiras, and P. Jarillo-Herrero, Nature **556**, 43 (2018).
- <sup>70</sup> Y. Cao, D. Chowdhury, D. Rodan-Legrain, O. Rubies-  
Bigordà, K. Watanabe, T. Taniguchi, T. Senthil, and  
P. Jarillo-Herrero, arXiv e-prints , arXiv:1901.03710  
(2019), arXiv:1901.03710 [cond-mat.str-el].
- <sup>71</sup> A. L. Sharpe, E. J. Fox, A. W. Barnard, J. Finney,  
K. Watanabe, T. Taniguchi, M. A. Kastner, and  
D. Goldhaber-Gordon, arXiv e-prints , arXiv:1901.03520  
(2019), arXiv:1901.03520 [cond-mat.mes-hall].